chemistry

Carbon Nanotubes Modified by BiMo Metal Oxides for Oxidative Dehydrogenation of 1-Butene to 1,3-Butadiene without Steam

Jiao Wu [1], Yu Liang [1], Gui Li [1] and Chao Wan [1,2,3,4,*]

[1] Anhui Province Key Laboratory of Coal Clean Conversion and High Valued Utilization, School of Chemistry and Chemical Engineering, Anhui University of Technology, Ma'anshan 243002, China; wujiao3366@outlook.com (J.W.); ly970130516@outlook.com (Y.L.); li970123@outlook.com (G.L.)

[2] Zhejiang Provincial Key Laboratory of Advanced Chemical Engineering Manufacture Technology, College of Chemical and Biological Engineering, Zhejiang University, 38 Zheda Road, Hangzhou 310027, China

[3] Jiangsu Key Laboratory of Advanced Catalytic Materials and Technology, Changzhou University, Changzhou 213164, China

[4] Anhui Haide Chemical Technology Co., Ltd., Ma'anshan 243002, China

[*] Correspondence: wanchao@zju.edu.cn or wanchao1219@hotmail.com

Abstract: Oxidative dehydrogenation (ODH) reaction has emerged as a promising route for converting 1-butene to value-added 1,3-butadiene (BD). However, the low BD selectivity of the current catalysts ($\leq 40\%$) and high steam input are now the challenge of this process. Here, we demonstrate the fabrication BiMo oxides immobilized on carbon nanotubes (BiMo/CNTs), employing the sol–gel method, as a novel catalyst for the ODH of 1-butene without steam in a fixed-bed reactor. The catalytic performances of BiMo/CNTs with different compositions in the absence of steam were investigated. When BiMo/CNTs at a molar ratio of 0.018 were employed in the ODH of 1-butene under reaction conditions of 440 °C, 1-butene/oxygen = 1/0.8, and no steam, the optimal BD yield was achieved as high as 52.2%. Under this reaction condition, the catalyst maintains good stability without steam after 10 h of reaction. This work not only promotes the application of carbon materials in oxidative dehydrogenation reaction, but also accelerates the production of 1,3-butadiene in a more economical way.

Keywords: 1-butene; 1,3-butadiene; oxidative dehydrogenation; BiMo/CNTs

1. Introduction

1,3-Butadiene (BD), an important raw material in the petrochemical industry and one of the most significant monomers for synthesis of coatings and synthetic rubber, plays a crucial role in the development of the chemical industry [1–3]. Nowadays, BD is mostly prepared by hydrocarbon steam cracking [4–6]. However, high energy consumption is invested in producing only low BD yield, thus restricting the development of the downstream industry of BD. The quest for a new butadiene production process is looming. Oxidative dehydrogenation (ODH) of 1-butene, which is mainly supplied from refinery waste gases, is a highly attractive process to produce 1,3-butadiene owing to its high yield and easy industrialization [7–10]. Therefore, designing more efficient catalysts and economical catalytic strategies to manufacture BD is still a challenging task.

Various catalysts, including noble metal catalysts and non-noble metal catalysts, have been widely used in the ODH of 1-butene [11–18]. Among them, noble-metal-free catalysts have received considerable attention due to their abundant reserves and low cost [19–21]. After several decades of extensive research, BiMo-based catalysts were regarded as one of the most effective catalysts in the ODH of 1-butene [21–23]. Cheng et al. reported a series of BiMo-based catalysts by introducing other metal component, such as

V, Co, and Ce, to improve the mobility of BiMo-based catalysts, thus enhancing the ODH performance [23–26]. Song et al. synthesized three types of pure BiMo oxides, including α-Bi$_2$Mo$_3$O$_{12}$, β-Bi$_2$Mo$_2$O$_9$, and γ-Bi$_2$MoO$_6$, and investigated the influence of phase in the ODH of 1-butene [26–28]. However, the above-mentioned BiMo-based catalysts demonstrate excellent catalytic performance in the ODH of 1-butene in the presence of steam, and the molar ratio of steam/1-butene is as high as 15. The introduction of water obviously increases the energy consumption, thus severely impeding the large-scale industrialization. Therefore, it is imperative to design a novel catalyst for promoting the ODH of 1-butene to BD without steam.

In recent years, carbon nanotubes (CNTs) have a wide range of applications [29,30]. Here, CNTs have found their applicability in the ODH of light hydrocarbons to olefins owing to the unique functional group structure on the surface [31–34]. Especially, Su et al. first employed CNTs as the ODH of n-butane to butenes and BD; high stability was maintained for as long as 100 h [35]. Su et al. further used acid-washed activated carbon in the ODH of 1-butene with a BD yield of 43% without steam [36]. Modified CNT catalysts, especially those loaded with oxides on the surface of CNTs, exhibit good catalytic activity and stability in the ODH of light hydrocarbons, mainly due to their stable structure and the concentration of oxygen-containing functional groups on the surface, which is favorable to improve the oxygen mobility of the catalyst and increase the conversion of the reactants [37–41]. It has been accepted that factors, such as the catalyst surface structure, elemental composition, and oxygen mobility, influence the catalytic performance of the catalyst. Recently, chromium oxides, phosphorus, and molybdenum oxides have been investigated to change the surface structure of CNTs, providing enough reactive sites to enhance the catalytic activity and stability of the catalyst [42–44]. However, to the best of our knowledge, no study about the combination of BiMo oxides and CNTs has been performed to improve the ODH reaction.

In this work, the loading of BiMo oxides on the surface of CNTs was constructed by the sol–gel method. A series of BiMo/CNTs with a different metal loading was employed in the ODH of 1-butene. The catalysts were further characterized by a series of techniques, such as XRD, XPS, TEM, and BET. Furthermore, the stability of the optimal BiMo/CNTs was extensively investigated in the absence of steam as well.
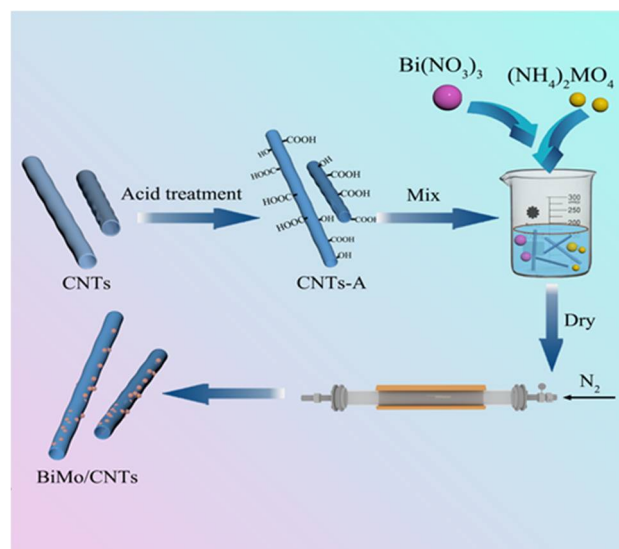
2. Experimental

2.1. Reagents and Materials

Carbon nanotubes (CNTs) were produced by Shenzhen nanoport Co., Ltd (Shenzhen, China). Nitric acid (HNO$_3$, AR), bismuth nitrate pentahydrate (Bi(NO$_3$)$_3$·5H$_2$O, AR), ammonium molybdate tetrahydrate ((NH$_4$)$_6$Mo$_7$O$_{24}$·4H$_2$O, AR), and ethanol (AR) were produced by Sinopharm Chemical Reagent Co., Ltd(Shanghai, China). Argon (99.999%) was produced by Hangzhou Jingong Gas Co., Ltd (Hangzhou, China). Purified water was produced by Wahaha Group Co., Ltd (Hangzhou, China).

2.2. Synthesis of Catalyst

The composite catalyst was prepared by the sol–gel method. In detail, 1 g of CNTs was added in 150 mL of 30% nitric acid, placing it in an oil bath with refluxing for 24 h at 140 °C. After cooling to room temperature, the solution was filtered and washed to neutrality, and the obtained samples were dried in an oven at 100 °C for 6 h to obtain the catalytic precursor. Further, 0.5 g of the catalytic precursor was stirred in an oil bath at 60 °C. A certain amount of bismuth nitrate and ammonium molybdate, respectively, were dissolved in a certain volume of ethanol solution to acquire two solutions, putting them dropwise simultaneously in the above catalyst precursor at a round-bottomed flask, mixing for 6 h. Subsequently, the temperature of the oil bath was raised to 90 °C, keeping the agitation until the above solution became viscous and uniform, and the resulting mixture was dried at 100 °C for 12 h. Finally, the solid compound was heated at 550 °C for 4 h with a heating rate of 5 °C·min^{-1} under an Ar atmosphere. Then, thoroughly cooling, these

samples were prepared and denoted as x(BiMo)/CNTs (x was the molar ratio of BiMo). And the molar ratio of Bi/Mo was 1:1. In brief, the catalyst was prepared by the sol–gel method using bismuth nitrate and ammonium molybdate as the precursor, as displayed in Scheme 1. The unsupported BiMo was prepared by a co-precipitation method with ammonium molybdate and bismuth nitrate as the precursors using an ammonia solution to accomplish the precipitation of the precursors.

Scheme 1. Schematic diagram of the synthesis of BiMo/CNTs.

2.3. Characterization of the Catalysts

The crystallinity of the prepared catalysts with different components was analyzed by an X-ray diffractometer (Shimadzu XRD). The wavelength of Cu Kα rays was 0.154 nm. The tube voltage was set to 40 kV. The tube current was 40 mA, the scanning range was range is 5°–80°, and the scanning step was 0.02°. The nitrogen adsorption and desorption tests were carried out on the sample by using a physical adsorption instrument (ASAP2020, Micromeritics, Norcross, GA, USA), and the specific surface area and pore volume of the sample were determined. Measured at −196 °C, the samples were degassed under vacuum at 200 °C for 6 h before the test. The surface composition of the catalyst was analyzed by X-ray photoelectron spectroscopy (XPS, Escalab 250Xi, Thermo Scientific, Waltham, MA, USA), and the X-ray source were Kα rays of Mg at a high voltage of 12 kV. An F-type high-resolution transmission electron microscope (TEM, JEOL JEM-2100, Tokyo, Japan) was used to analyze the morphology and element distribution of catalysts with different components.

2.4. Evaluation of Oxidative Dehydrogenation of 1-Butene

The catalytic evaluation of the composite catalyst includes catalyst loading, reaction, and product analysis. An amount of 1.5 g of catalyst was placed in a fixed-bed reactor (i.d. = 8 mm), and the catalyst was pretreated by flowing air stream at 440 °C for 1 h. The pretreatment was completed, the feed gas was introduced into it, the volume and flow rate were controlled, the reaction temperature was 440 °C, the ratio of butene to air was 1:4, and the total air velocity was 750 mL (g cat)$^{-1}$ h^{-1}. The analysis of the product means that the product is chromatographed at regular intervals. The chromatographic detection of the catalyst is performed by Kiyang gas chromatography (GC-9860) using a programmed ramp-up method for the analysis of the products.

3. Results and Discussion

Figure 1 shows the scanning transmission electron microscopy (STEM) of the (BiMo)/CNT catalysts and the distribution of the elements, from which it is evident that the elements

bismuth and molybdenum are uniformly distributed on the surface of the CNTs and are not associated with each other, but are mostly dispersed, confirming that the catalysts are mainly formed by the composite of the CNTs and the two metal oxides on their surface. In the evaluation process of comparing the catalysts for the oxidative dehydrogenation of butene, we found that the catalytic effect of the BiMo composite catalysts was significantly better than that of the pure single-component catalyst. Combined with the composite catalyst with the best catalytic effect, Figure 1 (0.018 (BiMo)/CNTs) indicates that in the process of dehydrogenation reaction, not a single component plays a role, but the synergistic effect of two BiMo components promotes a reaction.
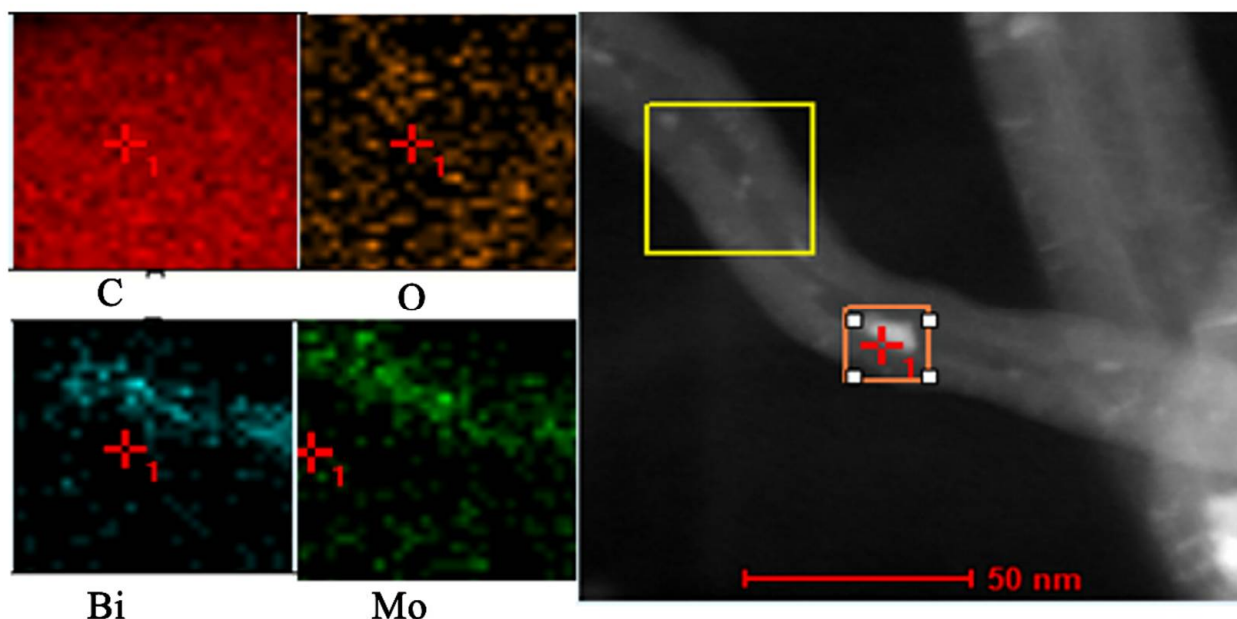

Figure 1. STEM images and elemental mapping of the elements O, C, Mo, and Bi of the 0.018 (BiMo)/CNTs catalyst.

A wide-angle X-ray diffraction (XRD) pattern was used to explore the x (BiMo)/CNT (x = 0, 0.006, 0.012, 0.018, 0.024) crystal structure of the sample, as shown in Figure 2a. The pure component catalysts containing Bi and Mo have apparent characteristic peaks. With the addition of the two components in different molar ratios, the spectrum shows visible peak changes. The characteristic peaks of Bi and Mo gradually intensified with increasing loadings of the two metals. Compared with the spectra of the pure components of Bi-containing (0.024Bi/CNTs) and Mo-containing (0.024Mo/CNTs) catalysts, the bismuth–molybdenum composite catalysts with different contents are formed by the composite of two components along with the formation of β-$Bi_2Mo_2O_9$. For 0.018 (BiMo)/CNTs, the 2θ centered at $27.2°$, $38.0°$, $39.6°$, and $48.7°$ can be ascribed to the (012), (104), (110), and (202) planes Bi (JCPDS No. 85-1329). An obvious peak at $27.2°$ may be attributable to the carbon (JCPDS No. 75-0444). Three peaks at $27.9°$, $31.8°$, and $33.1°$ can be attributed to β-$Bi_2Mo_2O_9$. Other three peaks at $26.0°$, $37.0°$, and $53.5°$ can be corresponded to MoO_2 (JCPDS No. 6-0135). However, for pure bismuth–molybdenum oxides, the samples were confirmed with only β-$Bi_2Mo_2O_9$ [20,21]. Combined with the different catalytic activities of different catalysts in the catalytic reaction process, the synthesized complexes contribute to the improvement of the catalytic reaction rate. The newly synthesized composite catalyst can promote the catalytic reaction.
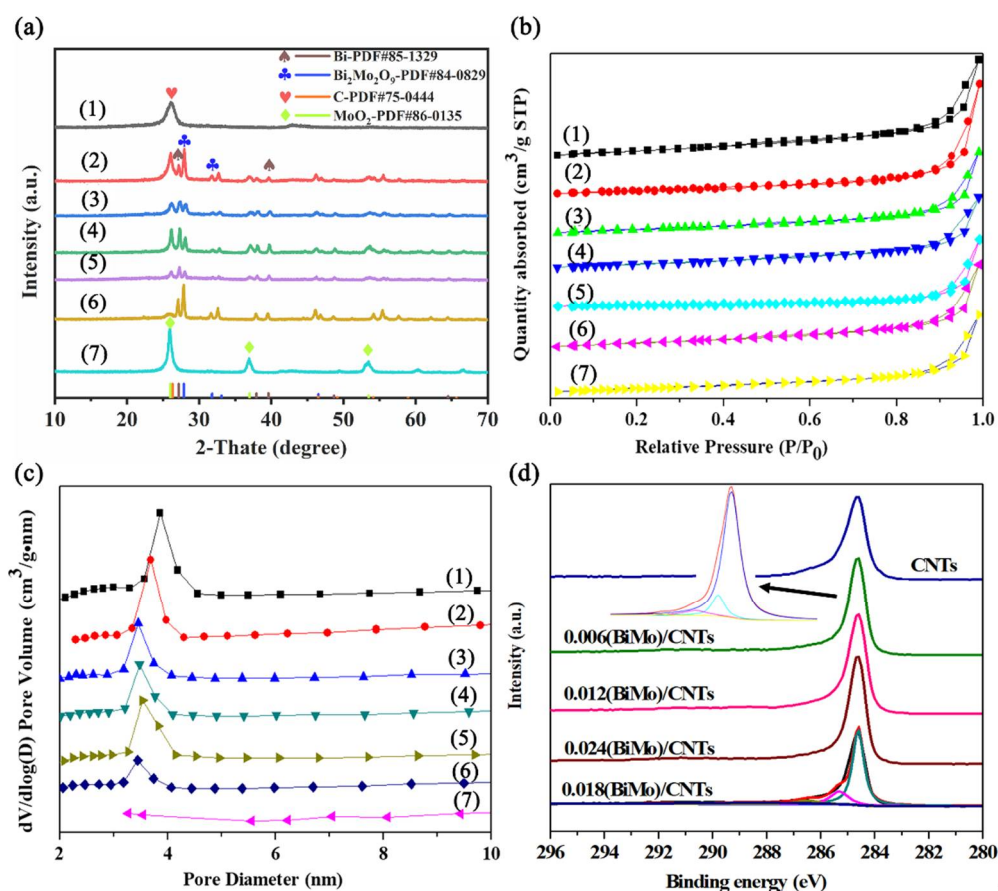
Figure 2. (**a**) XRD patterns of CNT catalysts with different compositions: (1) CNTs, (2) 0.006(BiMo)/CNTs, (3) 0.012(BiMo)/CNTs, (4) 0.018(BiMo)/CNTs, (5) 0.024(BiMo)/CNTs, (6) 0.024Bi/CNTs, and (7) 0.024Mo/CNTs; (**b**) N_2 adsorption–desorption isotherms of CNT catalysts with different compositions; (**c**) their pore size distributions: (1) CNTs, (2) 0.006(BiMo)/CNTs, (3) 0.012(BiMo)/CNTs, (4) 0.018(BiMo)/CNTs, (5) 0.024(BiMo)/CNTs, (6) 0.024Bi/CNTs, and (7) 0.024Mo/CNTs; (**d**) XPS C1s of different catalyst samples.

Figure 2b shows the N_2 adsorption–desorption isotherms of CNTs catalyst with different compositions. It can be seen from the figure that the material has an obvious mesoporous hysteresis loop, but the composite material is slightly different, which is distinct from that of pure CNTs. Compared with the curves of pure CNTs, it can be seen that the hysteresis loop of the new composite material is significantly smaller, and it can also be seen from the pore size distribution diagram that the pore size of the loaded material becomes smaller, from 4 nm to about 3.5 nm (Figure 2c). Table 1 shows the changes in a specific surface area and pore volume with different compositions. It can be seen from the table that compared with pure CNTs, the addition of Bi and Mo will reduce the specific surface area of the catalyst, but when the molar ratio of the two components gradually increases, the specific surface area of the catalyst will show an obvious downward trend. The change effect is more significant than that of pure components. The pore volume of the catalyst also decreases with the increase in the molar ratio of the two components, but the change is not clear.

Table 1. BET surface area, total pore volume, and catalytic performance of CNT catalysts with different compositions in the absence of steam.

Catalysts	Conversion (%)	Selectivity (%)	Yield (%)	S_{BET} (m$^2 \cdot$g^{-1})	Pore Volume (cm$^3 \cdot$g^{-1})
CNTs	40.9	59.8	24.5	107.9	0.33
BiMo	60	72	43.2	1.2	0.011
0.006(BiMo)/CNTs	67.2	58.6	39.4	86.7	0.37
0.012(BiMo)/CNTs	81.5	59.1	48.2	76.1	0.27
0.018(BiMo)/CNTs	86.7	60.2	52.2	75.1	0.24
0.024(BiMo)/CNTs	79.5	58.2	46.3	48.3	0.23
0.024Bi/CNTs	41.9	60.1	25.2	83.6	0.28
0.024Mo/CNTs	43.1	61.2	26.4	72.4	0.26

X-ray photoelectron spectroscopy (XPS) was further performed to investigate the chemical states of C elements with different metal ratios. The C 1s spectrum exhibits four distinct peaks at 284.6, 285.3, 286.5, and 288.3 eV in 0.018(BiMo/CNTs) in Figure 2d, attributed to the adventitious carbon, C–OH, C=O, and COOH, respectively. Among them, the area for COOH is far smaller than that for C–OH and C=O and can be ignored. According to the mechanism of the reaction [35,36], C=O as an electron donor is the main active site during the oxidative dehydrogenation reaction, and the butadiene generated during the reaction is retained as a reaction intermediate. Moreover, C–OH is pyrolyzed to generate C=O and H$_2$ in this reaction. Thus, the higher the ratio of C=O to C–O, the stronger the catalytic activity of the catalyst in the whole reaction process. Figure 3a shows the intensity ratios of some oxygen-containing functional groups for different catalysts. Specifically, with the increasing molar ratio of BiMo, the whole curve shows a parabolic change, which indicates that the C=O/C–O value of the pure component catalyst is lower than that of the composite catalyst in a certain proportion. The ratio of C=O/C–O has a great relationship with the catalytic activity of the corresponding catalyst. Therefore, 0.018(BiMo)/CNTs have perfect catalytic activity because of its high C=O to C–O ratio at 0.34. As displayed in Figure 3b, the yield of BD increased first and then decreased with the increase in metal composite ratio, the performance of the catalyst could reach the highest value in this system when the metal loading molar ratio is 0.018, and the yield of BD can reach the optimal value as high as 52.2% at 440 °C. However, the yields of BD for BiMo and CNTs are 43.2% and 24.5%, respectively. The corresponding conversions for these two catalysts are 60% and 40.9%, respectively. In combination with characterizations, it can be deduced that the interaction between metal oxides and surface functional groups promotes the oxidative dehydrogenation of 1-butene to BD. Compared with the reported literature about the oxidative dehydrogenation of 1-butene without steam [35,36], the 0.018(BiMo)/CNTs exhibited the optimal catalytic performance (Table 2). Combined with a similar curve change process presented in Figure 3a, it can be concluded that the superior catalytic activity of the catalyst with the composite metal loading molar ratio is closely related to the synergistic effect of the two metals.

Figure 3c,d shows the catalytic results of 0.018(BiMo)/CNTs and BiMo at 440 °C without steam. From Figure 3c, it can be seen that the composite catalysts maintain high activity and selectivity at a reaction time of 10 h, where the yield of butadiene remains at 50%. From Figure 3d, it can be seen that the catalytic activity of the BiMo component decreases significantly after 10 h of reaction, and the yield of BD decreases from 43.2% to 36.4%; moreover, the selectivity for BD decreases from 72% to 60%. Under the same reaction conditions, the composite catalyst performed excellently, with higher catalytic activity and selectivity, and the product yield was maintained at a high level. This can be attributed to the addition of composite metals to improve the oxygen mobility of the catalyst, and the synergistic effect of BiMo bimetals further promotes the performance of the catalyst during the reaction process. It can be concluded that the composite catalyst

exhibited superior catalytic performance in the absence of water compared with the pure component BiMo catalyst.
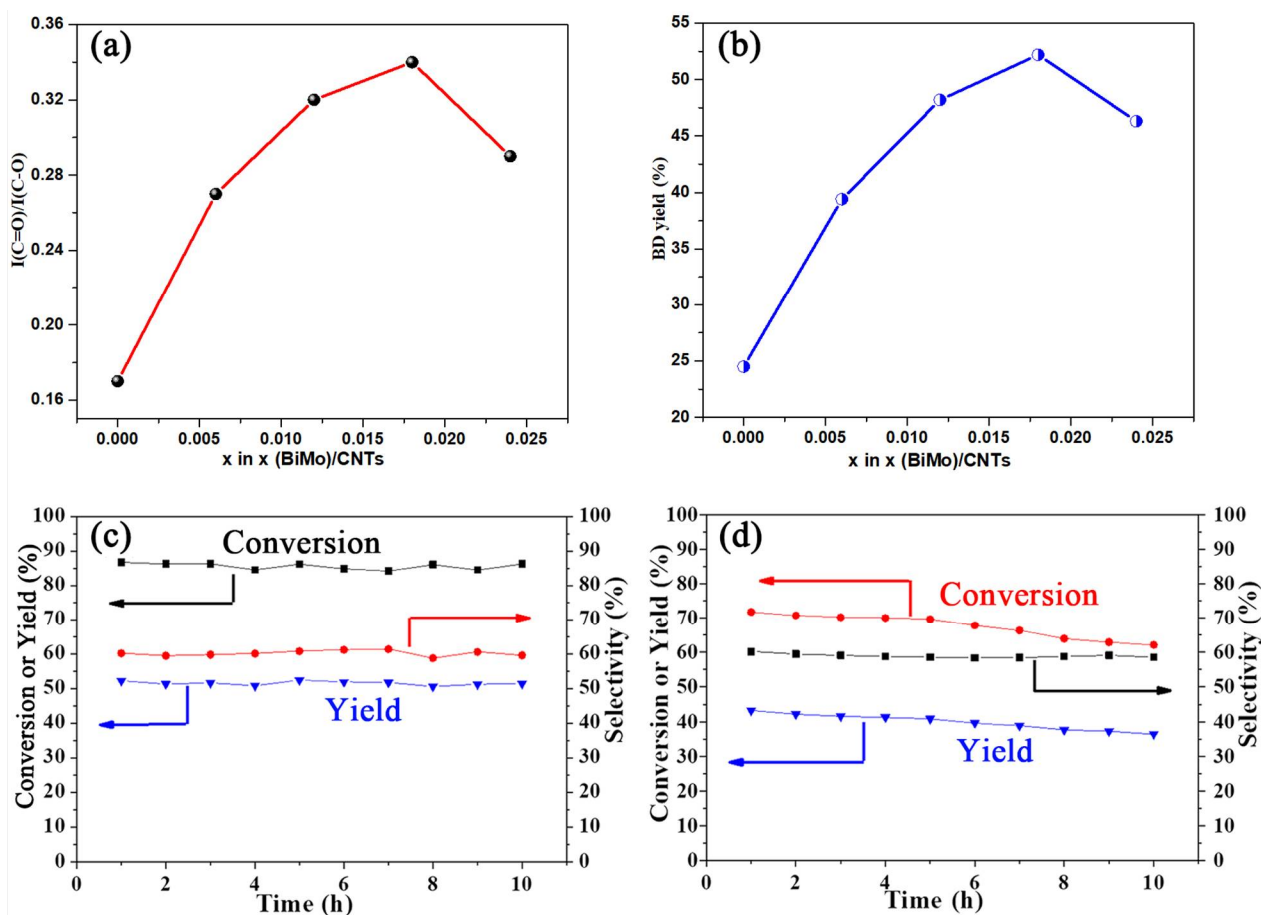

Figure 3. (**a**) $I(C=O)/I(C-O)$ of CNT catalysts in x(BiMo)/CNTs, (**b**) the relationship of BD yield with respect to x in x(BiMo)/CNTs without water, the catalytic performance without water in the ODH reaction: conversion, yield in BD, selectivity to BD and CO_2 for (**c**) 0.018 (BiMo)/CNTs (**d**) BiMo.

Table 2. Comparison of catalytic performances for different catalysts under no steam.

Catalysts	Conversion (%)	Selectivity (%)	Yield (%)	Ref.
0.018(BiMo)/CNTs	86.7	60.2	52.2	This work
CNTs	40.9	59.8	24.5	This work
P-o/CNTs	20	10	2	[35]
Activated-CNTs	72	59.7	43	[36]

4. Conclusions

In summary, we demonstrated a novel approach for the preparation of BiMo/CNTs by employing the sol–gel method. The introduction of the active components effectively improved the oxygen mobility of the catalysts and further enhanced the catalytic performance, enabling the catalysts to exhibit excellent catalytic activity in the ODH of 1-butene to BD in the absence of steam. The best catalytic activity was achieved at a metal molar ratio of 0.018, with a maximum BD yield of 52.2%. Compared with BiMo oxides, 0.018(BiMo)/CNTs exhibited a more obvious catalytic stability without steam. Our future aims in this scope of investigation focuses on designing the high-performance catalysts and promoting the large-scale application of BD production without steam. This work will guide the construction of the catalysts based on the advantages of CNTs and metal oxides and could be extended to other reactions.

Institutional Review Board Statement: Not applicable.

Informed Consent Statement: Not applicable.

Data Availability Statement: The data presented in this study are available on request from the corresponding author.

Conflicts of Interest: The authors declare that they have no conflict of interest.

Sample Availability: Samples of the compounds are available from the authors.

References

1. Jung, J.C.; Lee, H.; Song, I.K. Production of 1,3-butadiene from C_4 raffinate-3 through oxidative dehydrogenation of n-butene over bismuth molybdate catalysts. *Catal. Surv. Asia* **2009**, *13*, 78–93. [CrossRef]

2. Liu, L.L.; Zhou, X.J.; Guo, L.X.; Yan, S.J.; Li, Y.J.; Jiang, S.; Tai, X.S. Bimetallic Au–Pd alloy nanoparticles supported on MIL-101(Cr) as highly efficient catalysts for selective hydrogenation of 1,3-butadiene. *RSC Adv.* **2020**, *10*, 33417–33427. [CrossRef]

3. Zeng, T.Q.; Sun, G.; Miao, C.X.; Yan, G.; Ye, Y.C.; Yang, W.M.; Sautet, P. Stabilizing oxidative dehydrogenation active sites at high temperature with steam: $ZnFe_2O_4$-catalyzed oxidative dehydrogenation of 1-butene to 1,3-butadiene. *ACS Catal.* **2020**, *10*, 12888–12897. [CrossRef]

4. Gao, M.X.; Zhang, M.H.; Li, Y.H. Transformation of bioethanol to 1,3-butadiene and other bulk chemicals over the surface of Mg–Al catalysts. *RSC Adv.* **2017**, *7*, 26935–26942. [CrossRef]

5. Park, J.H.; Shin, C.H. Oxidative dehydrogenation of butenes to butadiene over Bi-Fe-Me (Me = Ni, Co, Zn, Mn and Cu) -Mo oxide catalysts. *J. Ind. Eng. Chem.* **2015**, *21*, 683–688. [CrossRef]

6. Li, X.Y.; Cheng, D.G.; Chen, F.Q.; Zhan, X.L. Dual bed catalyst system for oxidative dehydrogenation of mixed-butenes: A synergistic mechanism. *Zhejiang Univ. Sci. A* **2017**, *18*, 225–233. [CrossRef]

7. Sobolev, V.I.; Koltunov, K.Y.; Zenkovets, G.A. Oxidative dehydrogenation of 1-butene to 1,3-butadiene over a multicomponent bismuth molybdate catalyst: Influence of C_3-C_4 hydrocarbons. *Catal. Lett.* **2017**, *147*, 310–317. [CrossRef]

8. Kiyokawa, T.; Hagihara, T.; Ikenaga, N. Oxidative dehydrogenation of n-butene with V–Mg complex oxide with added trivalent metal oxide. *ChemistrySelect* **2019**, *4*, 906–913. [CrossRef]

9. Liu, X.; Duan, L.H.; Yang, W.S.; Zhu, X.F. Oxidative dehydrogenation of n-butane to butenes on Mo-doped VMgO catalysts. *RSC Adv.* **2017**, *7*, 34131–34137. [CrossRef]

10. Yan, W.J.; Kouk, Q.Y.; Luo, J.Z.; Liu, Y.; Borgna, A. Catalytic oxidative dehydrogenation of 1-butene to 1,3-butadiene using CO_2. *Catal. Commun.* **2014**, *46*, 208–212. [CrossRef]

11. Dasireddy, V.D.; Huš, M.; Likoza, B. Effects of Pt_0-PtO_x particle size on 1-butene oxidative dehydrogenation to 1,3-butadiene using CO_2 as soft oxidant. *Catal. Sci. Technol.* **2017**, *7*, 3291–3302. [CrossRef]

12. Yan, B.; Wang, B.L.; Wang, L.Y.; Jiang, T. Ce-doped mesoporous alumina supported Fe-based catalyst with high activity for oxidative dehydrogenation of 1-butene using CO_2 as soft oxidant. *J. Porous Mater.* **2019**, *26*, 1269–1277. [CrossRef]

13. Furukawa, S.; Endo, M.; Komatsu, T. Bifunctional catalytic system effective for oxidative dehydrogenation of 1-butene and n-butane using Pd-based intermetallic compounds. *ACS Catal.* **2014**, *4*, 3533–3542. [CrossRef]

14. Kiyokawa, T.; Ikenaga, N. Oxidative dehydrogenation of but-1-ene with lattice oxygen in ferrite catalysts. *Appl. Catal. A Gen.* **2017**, *536*, 97–103. [CrossRef]

15. Li, X.Y.; Cheng, D.G.; Zhao, Z.J.; Chen, F.Q.; Gong, J.L. Temperature-induced deactivation mechanism of $ZnFe_2O_4$ for oxidative dehydrogenation of 1-butene. *React. Chem. Eng.* **2017**, *2*, 215–225. [CrossRef]

16. Yang, B.Y.; Liu, L.; Zou, G.J.; Luo, X.; Zhu, H.L.; Xu, S. The roles of $ZnFe_2O_4$ and α-Fe_2O_3 in the biphasic catalyst for the oxidative dehydrogenation of n-butene. *J. Catal.* **2020**, *381*, 70–77. [CrossRef]

17. Wan, C.; Cheng, G.D.; Chen, F.Q.; Zhan, X.L. Oxidative dehydrogenation of 1-butene over vanadium modified bismuth molybdate catalyst: An insight into mechanism. *RSC Adv.* **2015**, *5*, 42609–42615. [CrossRef]

18. Park, J.H.; Noh, H.; Park, J.W.; Row, K.H.; Jung, K.D.; Shin, C.H. Oxidative dehydrogenation of n-butenes to 1,3-butadiene over BiMoFe$_{0.65}$P$_x$ catalysts: Effect of phosphorous contents. *Res. Chem. Intermed.* **2011**, *37*, 1125–1134. [CrossRef]

19. Yan, B.; Wang, L.Y.; Wang, B.L.; Alam, F.; Xiao, Z.Z.; Li, J.; Jiang, T. Constructing a high-efficiency iron-based catalyst for carbon dioxide oxidative dehydrogenation of 1-butene: The role of oxygen mobility and proposed reaction mechanism. *Appl. Catal. A Gen.* **2019**, *572*, 71–79. [CrossRef]

20. Jung, J.C.; Lee, H.; Kim, H.; Chung, Y.M.; Kim, T.J.; Lee, S.J.; Oh, S.H.; Kim, Y.S.; Song, I.K. A synergistic effect of α-Bi$_2$Mo$_3$O$_{12}$ and γ-Bi$_2$MoO$_6$ catalysts in the oxidative dehydrogenation of C$_4$ raffinate-3 to 1,3-butadiene. *J. Mol. Catal. A Chem.* **2007**, *271*, 261–265. [CrossRef]

21. Jung, J.C.; Lee, H.; Kim, H.; Chung, Y.M.; Kim, T.J.; Lee, S.J.; Oh, S.H.; Kim, Y.S.; Song, I.K. Unusual catalytic behavior of β-Bi$_2$Mo$_2$O$_9$ in the oxidative dehydrogenation of n-butene to 1,3-butadiene. *J. Mol. Catal. A Chem.* **2007**, *264*, 237–240. [CrossRef]

22. Park, J.H.; Shin, C.H. Influence of phosphorous addition on Bi$_3$Mo$_2$Fe$_1$ oxide catalysts for the oxidative dehydrogenation of 1-butene. *Korean J. Chem. Eng.* **2016**, *33*, 823–830. [CrossRef]

23. Wan, C.; Cheng, G.D.; Chen, F.Q.; Zhan, X.L. Effects of zirconium content on the catalytic performance of BiMoZr$_x$ in the oxidative dehydrogenation of 1-butene to 1,3-butadiene. *J. Chem. Technol. Biot.* **2016**, *91*, 353–358. [CrossRef]

24. Wan, C.; Cheng, G.D.; Chen, F.Q.; Zhan, X.L. The role of active phase in Ce modified BiMo catalysts for oxidative dehydrogenation of 1-butene. *Catal. Today* **2016**, *264*, 180–184. [CrossRef]

25. Wan, C.; Cheng, G.D.; Chen, F.Q.; Zhan, X.L. Characterization and kinetic study of BiMoLa$_x$ oxide catalysts for oxidative dehydrogenation of 1-butene to1,3-butadiene. *Chem. Eng. Sci.* **2015**, *135*, 553–558. [CrossRef]

26. Jung, J.C.; Lee, H.W.; Park, D.R.; Seo, J.G.; Song, I.K. Effect of calcination temperature on the catalytic performance of γ-Bi$_2$MoO$_6$ in the oxidative dehydrogenation of n-butene to 1,3-butadiene. *Catal. Lett.* **2009**, *131*, 401–405. [CrossRef]

27. Jung, J.C.; Kim, H.; Choi, A.S.; Chung, Y.M.; Kim, T.J.; Lee, S.J.; Oh, S.H.; Song, I.K. Effect of nickel precursor on the catalytic performance of Ni/Al$_2$O$_3$ catalysts in the hydrodechlorination of 1,1,2-trichloroethane. *J. Mol. Catal. A* **2006**, *256*, 178–183.

28. Jung, J.C.; Lee, H.; Seo, J.G.; Park, S.Y.; Chung, Y.M.; Kim, T.J.; Lee, S.J.; Oh, S.H.; Kim, Y.S.; Song, I.K. Oxidative dehydrogenation of n-butene to 1,3-butadiene over multicomponent bismuth molybdate (M^{II}$_9$Fe$_3$Bi$_1$Mo$_{12}$O$_{51}$) catalysts: Effect of divalent metal (M^{II}). *Catal. Today* **2009**, *141*, 325–329. [CrossRef]

29. Tabani, H.; Bameri, A.E.; Abedi, H.; Hatefi, R.; Gorjizadeh, A.; Moghaddam, A.Z. Introduction of nitrogen doped graphene nanosheets as efficient adsorbents for nitrate removal from aqueous samples. *J. Environ. Health. Sci. Eng.* **2021**, *19*, 1875–1886. [CrossRef]

30. Tabani, H.; Khodaei, K.; Moghaddam, A.Z.; Alexovič, M.; Movahed, S.K.; Zare, F.D.; Dabiri, M. Introduction of graphene-periodic mesoporous silica as a new sorbent for removal: Experiment and simulation. *Res. Chem. Intermed.* **2019**, *45*, 1795–1813. [CrossRef]

31. Wang, K.; Lu, Z.J.; Li, Y.Z.; Wang, S.Q.; Cao, Y.L. Interfacial engineering of bimetallic carbide and cobalt encapsulated in nitrogen-doped carbon nanotubes for electrocatalytic oxygen reduction. *ChemSusChem* **2020**, *13*, 5539–5548. [CrossRef] [PubMed]

32. Wan, C.; Sun, L.; Xu, L.X.; Cheng, D.G.; Chen, F.Q.; Zhan, X.L.; Yang, Y.R. Novel NiPt alloy nanoparticle decorated 2D layered g-C$_3$N$_4$ Nanosheets: A highly efficient catalyst for hydrogen generation from hydrous hydrazine. *J. Mater. Chem. A* **2019**, *7*, 8798–8804. [CrossRef]

33. Zhong, B.; Huang, R.; Su, D.S.; Liu, H.Y. Effect of graphitization of oxygen-modified carbon nanotubes in selective oxidation of acrolein. *Catal. Today* **2019**, *330*, 142–148. [CrossRef]

34. Wen, G.D.; Diao, J.Y.; Wu, S.C.; Yang, W.M.; Schlögl, R.; Su, D.S. Acid properties of nanocarbons and their application in oxidative dehydrogenation. *ACS Catal.* **2015**, *5*, 3600–3608. [CrossRef]

35. Zhang, J.; Liu, X.; Blume, R.; Zhang, A.H.; Schlögl, R.; Su, D.S. Surface-modified carbon nanotubes catalyze oxidative dehydrogenation of n-butane. *Science* **2008**, *322*, 73–77. [CrossRef]

36. Liu, X.; Su, D.S.; Schlögl, R. Oxidative dehydrogenation of 1-butene to butadiene over carbon nanotube catalysts. *Carbon* **2008**, *46*, 547–549. [CrossRef]

37. Chernyak, S.A.; Kustov, A.L.; Stolbov, D.N.; Tedeeva, M.A.; Isaikina, O.Y.; Maslakov, K.I.; Usol'tseva, N.V.; Savilov, S.V. Chromium catalysts supported on carbon nanotubes and graphene nanoflakes for CO$_2$-assisted oxidative dehydrogenation of propane. *Appl. Surf. Sci.* **2022**, *578*, 152099. [CrossRef]

38. Wan, C.; Zhou, L.; Xu, S.M.; Jin, B.Y.; Ge, X.; Qian, X.; Xu, L.X.; Chen, F.Q.; Zhan, X.L.; Yang, Y.R. Defect engineered mesoporous graphitic carbon nitride modified with AgPd nanoparticles for enhanced photocatalytic hydrogen evolution from formic acid. *Chem. Eng. J.* **2022**, *429*, 132388. [CrossRef]

39. Zhang, M.Y.; Liu, L.; Lu, S.; Xu, L.X.; An, Y.; Wan, C. Facile fabrication of NiPt/CNTs as an efficient catalyst for hydrogen production from hydrous hydrazine. *ChemistrySelect* **2019**, *4*, 10494–10500. [CrossRef]

40. Wan, C.; Zhou, L.; Sun, L.; Xu, L.X.; Cheng, D.G.; Chen, F.Q.; Zhan, X.L.; Yang, Y.R. Boosting visible-light-driven hydrogen evolution from formic acid over AgPd/2D g-C$_3$N$_4$ nanosheets Mott-Schottky photocatalyst. *Chem. Eng. J.* **2020**, *396*, 125229. [CrossRef]

41. Shi, L.; Qi, W.; Liu, W.; Yan, P.Q.; Li, F.; Sun, J.M.; Su, D.S. Carbon nitride modified nanocarbon materials as efficient non-metallic catalysts for alkane dehydrogenation. *Catal. Today* **2018**, *301*, 48–54. [CrossRef]

42. Hu, Z.P.; Chen, C.; Ren, J.T.; Yuan, Z.Y. Direct dehydrogenation of propane to propylene on surface-oxidized multiwall carbon nanotubes. *Appl. Catal. A Gen.* **2018**, *559*, 85–93. [CrossRef]

43. Han, Z.F.; Xue, X.L.; Wu, J.M.; Lang, W.Z.; Guo, Y.J. Preparation and catalytic properties of mesoporous nV-MCM-41 for propane oxidative dehydrogenation in the presence of CO_2. *Chin. J. Catal.* **2018**, *39*, 1099–1109. [CrossRef]

44. Zhang, S.Y.; Gao, Y.Y.; Zhang, Z.B.; Gu, T.; Liang, X.B.; Wang, L.Z. Research Progress on Functional Properties of Novel High-Entropy Metallic Glasses. *Chin. J. Rare Met.* **2021**, *45*, 717–727.